bioRxiv preprint doi: https://doi.org/10.1101/2023.07.16.549234; this version posted July 18, 2023. The copyright holder for this preprint (which was not certified by peer review) is the author/funder. All rights reserved. No reuse allowed without permission.

An In-Silico Testbed for Fast and Accurate MR Labeling of Orthopaedic Implants

GREGORY M NOETSCHER[1*], PETER J. SERANO[2,1*], MARC HORNER[2], ALEXANDER PROKOP[3], JONATHAN HANSON[4], KYOKO FUJIMOTO[5], JAMES E. BROWN[6], ARA NAZARIAN[7], JEROME ACKERMAN[8,9], SERGEY N MAKAROFF[1,9]

1. Electrical & Computer Eng. Dept. Worcester Polytechnic Institute, Worcester MA 01609-2280 USA, gregn@wpi.edu
2. Ansys, Inc., 2600 Ansys Drive, Canonsburg, PA 15317 USA, pete.serano@ansys.com
3. Dassault Systèmes Deutschland GmbH, Bad Nauheimer Str. 19, 64289 Darmstadt, Germany, alexander.prokop@3ds.com
4. Neva Electromagnetics, LLC, 1010 Main St., Holden, MA 01520, jonathan.hanson@nevaem.com
5. GE HealthCare, 500 W Monroe Street, Chicago, IL, 60661 USA, kyoko.fujimoto@ge.com
6. Micro Systems Engineering, Inc., an affiliate of Biotronik, 6024 Jean Road, Lake Oswego, OR 97035 USA, james.brown@biotronik.com
7. Musculoskeletal Translational Innovation Initiative, Department of Orthopedic Surgery, Beth Israel Deaconess Medical Center and Harvard Medical School, 330 Brookline Ave, RN123, Boston, MA, 02215 USA, anazaria@bidmc.harvard.edu
8. Harvard Medical School, Boston, MA 02115 USA
9. Athinoula A Martinos Center for Biomed. Imaging, Massachusetts General Hospital 149 13th St. Charlestown, MA 02129 USA, jlackerman@mgh.harvard.edu

*BOTH FIRST AUTHORS EQUALLY CONTRIBUTED TO THE PAPER

bioRxiv preprint doi: https://doi.org/10.1101/2023.07.16.549234; this version posted July 18, 2023. The copyright holder for this preprint (which was not certified by peer review) is the author/funder. All rights reserved. No reuse allowed without permission.

ABSTRACT

One limitation on the ability to monitor health in older adults using Magnetic Resonance (MR) imaging is the presence of implants, where the prevalence of implantable devices (orthopedic, cardiac, neuromodulation) increases in the population, as does the pervasiveness of conditions requiring MRI studies for diagnosis (musculoskeletal diseases, infections, or cancer). The present study describes a novel multiphysics implant modeling testbed using the following approaches with two examples:

- an *in-silico* human model based on the widely available Visible Human Project (VHP) cryo-section dataset;
- a finite element method (FEM) modeling software workbench from Ansys (Electronics Desktop/Mechanical) to model MR radio frequency (RF) coils and the temperature rise modeling in heterogeneous media.

The *in-silico* VHP Female model (250 parts with an additional 40 components specifically characterizing embedded implants and resultant surrounding tissues) corresponds to a 60-year-old female with a body mass index (BMI) of 36. The testbed includes the FEM-compatible *in-silico* human model, an implant embedding procedure, a generic parameterizable MRI RF birdcage two-port coil model, a workflow for computing heat sources on the implant surface and in adjacent tissues, and a thermal FEM solver directly linked to the MR coil simulator to determine implant heating based on an MR imaging study protocol. The primary target is MR labeling of large orthopaedic implants. The testbed has very recently been approved by the US Food and Drug Administration (FDA) as a medical device development tool (MDDT) for 1.5 T orthopaedic implant examinations.

KEYWORDS:

Orthopaedic Implants
MR imaging studies
Temperature rise
MR Safety/MR Labeling
In-silico computational testbed
Multiphysics modeling

bioRxiv preprint doi: https://doi.org/10.1101/2023.07.16.549234; this version posted July 18, 2023. The copyright holder for this preprint (which was not certified by peer review) is the author/funder. All rights reserved. No reuse allowed without permission.

1. INTRODUCTION

One limitation on the ability to monitor health in older adults using Magnetic Resonance (MR) imaging studies is the presence of implants, where the prevalence of implantable devices (orthopedic, cardiac, neuromodulation) increases in the population, as does the pervasiveness of conditions requiring MRI studies for diagnosis (musculoskeletal conditions, infections, or cancer). In 2020, 26% of the US population over 65 was estimated to carry a large joint or spinal implant [1]. Simultaneously, 12.6 million patients over 65 who carry orthopedic or cardiac implants will need an MR study within 10 years, according to an estimate in 2020 [1] with this number expected to rise. Similarly, over 70% of the estimated 3 million pacemakers in the US are implanted in patients older than 65 [2],[3], where approximately 20% of these patients will need an MR study within 12 months of device implantation [4].

Terms to be used to label MR information for medical devices – implants – include *MR safe*, *MR conditiona*l, and *MR unsafe* [5],[6],[7],[8]. MR safe items are nonconducting, nonmetallic, and nonmagnetic items, such as a plastic Petri dish [8]. MR unsafe items include in particular ferromagnetic materials [8]; they should not enter the MR scanner room [6]. All other devices that contain any metallic components, such as titanium, (regardless of ferromagnetism) are *MR conditional* and will need to be evaluated and labeled for RF-induced heating, image artifact, force, and torque [5]. For the corresponding labeling icons, see [6].

MR conditional implants may safely enter the MR scanner room only under the very specific conditions provided in the labeling. Patients should not be scanned unless the device can be positively identified as MR conditional and the conditions for safe use are met [6]. When present, information about expected temperature rise and artifact extent may inform the risk/benefit decision of whether or not a patient should undergo an MR examination [6].

Given the large numbers of implants subject to conditional labeling, the number of cleared FDA 510(k) submissions for orthopedic implantable devices with MR labeling has been growing exponentially since 2014 [9], approaching 100 in 2019 [9]. However, practical testing is limited by constraints related to cost and resources, including testing tools [9]. As a result, a number of implants have been labeled "*MR Not Evaluated*", which precludes patients' access to MR imaging procedures [9]. Other implants may be labeled too restrictively [1], limiting patient access to MR imaging [10]. When estimating combined data from [1],[9],[10],[12], up to two million elderly patients in the US are potentially affected by MR labeling uncertainty.

Presumably, the most important consequence of this uncertainty is restricting general access to MR imaging studies for patients with implants. This also prevents the use of MR imaging for better soft tissue monitoring in the vicinity of implants. A prime example of the latter is

bioRxiv preprint doi: https://doi.org/10.1101/2023.07.16.549234; this version posted July 18, 2023. The copyright holder for this preprint (which was not certified by peer review) is the author/funder. All rights reserved. No reuse allowed without permission.

periprosthetic joint infection following total hip replacement surgery, which occurs in only 1%–2% of primary arthroplasties [14],[15] but in up to 30% of revision arthroplasties [15]. This form of infection occurs due to mechanical loosening and dislocation, currently the most common causes for revision of total hip arthroplasty in the United States [16]. Periprosthetic joint infection related mortality is approaching 5-8% at one year [14]. Presently, X-rays and other methods are used for diagnosis [17], but results of MR imaging with metal artifact reduction were recently shown to be the most accurate tool in the diagnosis of several biomarkers of periprosthetic hip joint infection [15],[18].

One major safety concern, relevant to both passive and active implants, is implant heating within MR radiofrequency and gradient coils [5]. Along with the required yet not entirely anatomical ASTM phantom test [5],[19], numerical simulations with virtual human models generate accurate predictions of temperature rise [20],[21],[22],[23],[24],[25],[26] accepted by the FDA [26]. The electromagnetic and thermal simulation algorithms based on finite element, finite difference, and boundary element methods are reasonably well developed [27],[28],[31],[32]. However, accessible, full body, detailed anatomical virtual human models reflecting major age, sex, race, and obesity variations are severely lacking. Their creation is a long, tedious, and labor-intensive process. Even today, it requires manual and semiautomatic supervised segmentation of full body MR images, surface mesh reconstruction, mesh intersection resolution, software compatibility and robustness testing, and finally examination of hundreds of different body compartments by anatomical experts.

An excellent collection of *in-silico* human body models intended for this purpose is the Virtual Population, a product of the IT'IS Foundation [26],[29] widely used in both industrial and academic applications. While this population has many highly detailed body models, it is relatively homogeneous: reasonably fit, younger Caucasian European subjects, representing a comparatively limited subsection of human anatomy and physiology. Although three obese models were added in 2023 [30] , two of the three are not truly anatomical and were obtained via morphing (the 'Fats' model being the exception). Also, while models are available for purchase and for research purposes, no background MRI data enabling independent tissue structure verification have been made publicly available for this population set.

The present study describes a complete ready-to-use implant modeling testbed for RF heating based on

(i) an *in-silico* human model constructed from the widely available Visible Human Project (VHP) [34],[35] cryo-section dataset;

bioRxiv preprint doi: https://doi.org/10.1101/2023.07.16.549234; this version posted July 18, 2023. The copyright holder for this preprint (which was not certified by peer review) is the author/funder. All rights reserved. No reuse allowed without permission.

(ii) a FEM modeling software workbench from Ansys HFSS (Electronics Desktop) to model the physical phenomena of a MR RF coil and corresponding temperature rise in heterogeneous media.

The *in-silico* VHP Female model (250 anatomical structures with additional 40 components specifically characterizing embedded implants [31]) characterizes a 60-year-old female subject with a body mass index (BMI) of 36. The open-source version of this model [13] has over 600 registered users from both industry and academia worldwide. The testbed includes the *in-silico* model, an implant embedding procedure, a generic parameterizable MR RF birdcage two-port coil model, a workflow for computing heat sources on the implant surface and neighboring tissues, and a thermal FEM solver directly linked to the MR coil simulator to estimate implant heating based on an MR imaging protocol. The primary target is MR labeling of large orthopaedic implants. The testbed has recently been approved by the US Food and Drug Administration (FDA) as a medical device development tool (MDDT) [11] for 1.5 T orthopaedic implant examinations. We also present two simple application examples pertinent to choosing an appropriate MR imaging protocol for a particular orthopaedic implant as well as validation against measurements of the heading of an ablation needle in bovine liver.

2. Materials and Methods

2.1 *In silico*-human model and implant embedding procedure

Fig. 1 shows surface CAD meshes for the VHP-Female model [27],[31] (with some muscles removed for clarity) and examples of passive femoral implants embedded into the model. The corresponding physical femoral implants are shown on the top right of the figure.

The implant registration enforces an anatomically correct implant position, and a certain part of the bone matter (cortical and/or trabecular) to be removed as necessary. A semiautomatic implant registration algorithm requiring limited user intervention has been employed based on the principal idea to use at least two anchor nodes per implant: a fixed node and a floating node. The floating anchor node is a vertex of the implant mesh belonging to a certain curve, say, the long axis of the bone. The fixed anchor node is a joint coincident vertex of the femur mesh and the implant mesh. These nodes define the proper implant position given the bone model and a cost function, with a “best fit” based on a mesh intersection check and the signed normal distances between implant/bone boundaries. An additional criterion involves the minimum required thickness of the cortical bone matter with an embedded implant.

bioRxiv preprint doi: https://doi.org/10.1101/2023.07.16.549234; this version posted July 18, 2023. The copyright holder for this preprint (which was not certified by peer review) is the author/funder. All rights reserved. No reuse allowed without permission.

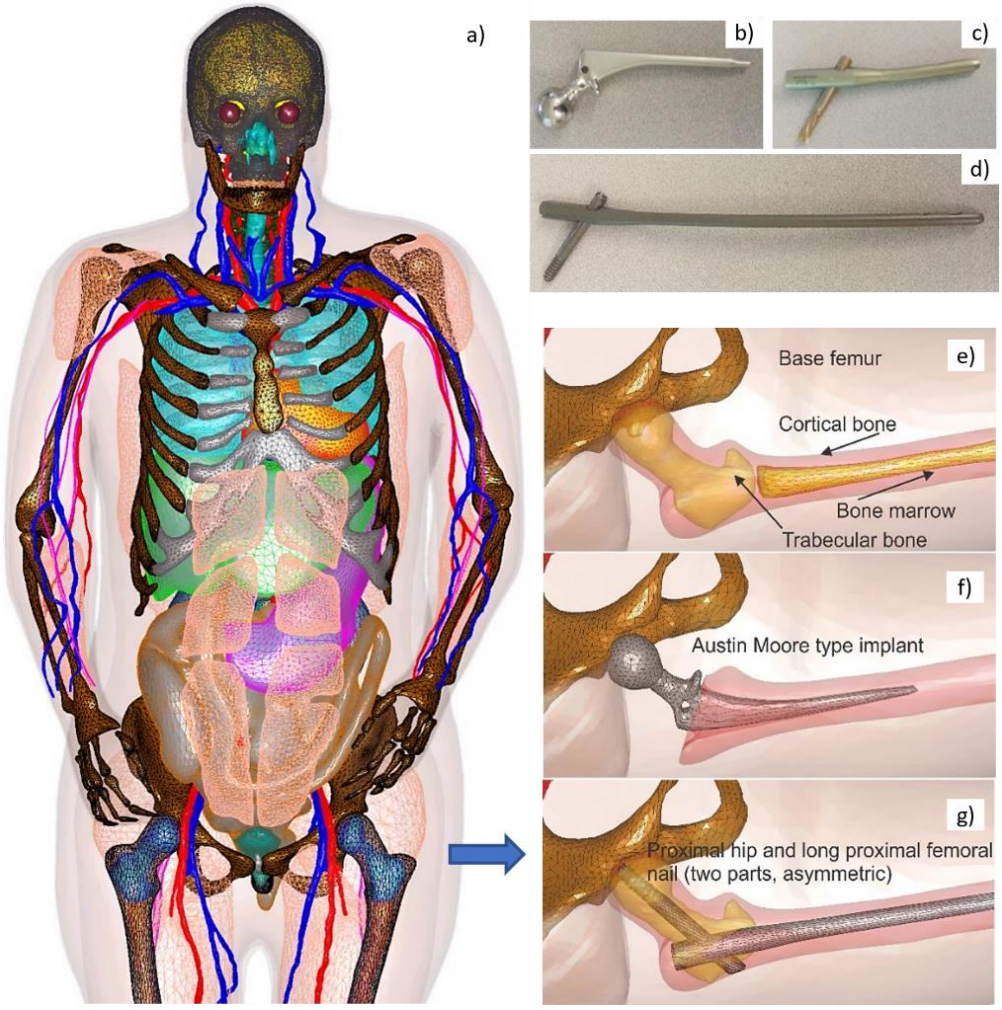

Fig. 1. Left a) – surface CAD meshes for the VHP-Female model (with some muscles removed for purposes of visualization); and right – examples of passive femoral implants embedded into the model. Figs. 1b-d at top right – physical femoral implants; Figs. 1e-g at center and bottom – anatomically justified CAD realization within the virtual human VHP-Female. An Austin Moore implant is shown in Fig. 1b; a short proximal femoral nail with the proximal hip (a large femoral neck screw) is given in Fig. 1c; a long proximal femoral nail with the proximal hip is presented in Fig. 1d.

2.2 Computation of heat sources due to microwave absorption in MR RF coils

A generic, parameterized, and tunable MR RF birdcage two-port coil model (high-, low-, or bandpass), at 64 MHz (1.5 T) with a variable number of rungs was implemented in Ansys Electronics Desktop (Ansys HFSS, Fig. 2a). This model is used to compute heat sources – either specific absorption rate (SAR) in W/kg, or power loss density (PLD) in W/m^3 at any point in the body, including on the surface of the implants (Figs. 2b and c [33]). The *in-silico* model with the implant(s) can be positioned at any appropriate landmark.

bioRxiv preprint doi: https://doi.org/10.1101/2023.07.16.549234; this version posted July 18, 2023. The copyright holder for this preprint (which was not certified by peer review) is the author/funder. All rights reserved. No reuse allowed without permission.

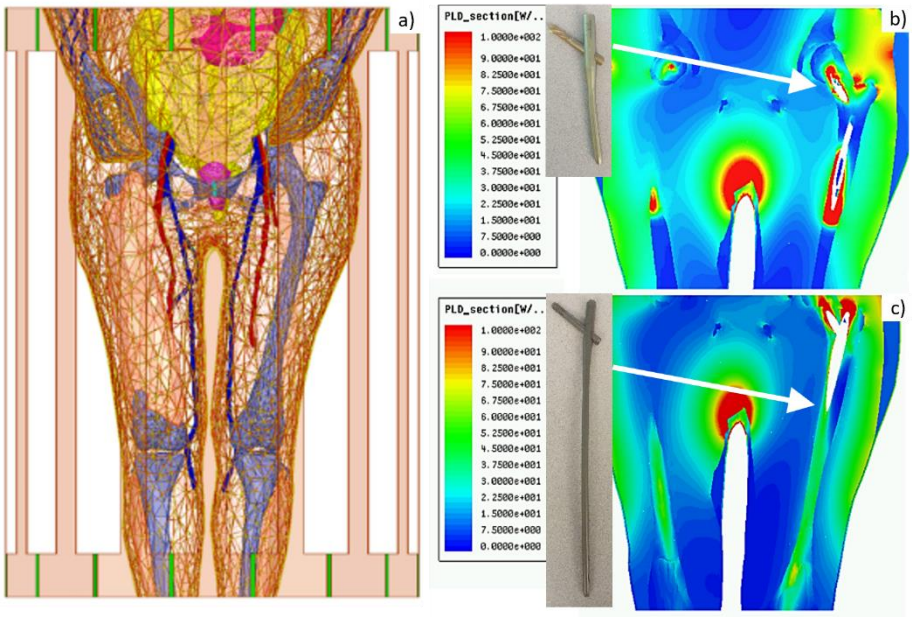

Fig. 2. Left – VHP-Female computational phantom positioned within a 1.5 T MRI birdcage coil at the abdominal landmark. Right - power loss density in W/m^3 in the coil for the b) Austin Moore and c) femoral nail implants.

2.3 Determination of implant temperature rise as a function of scan time

An Ansys FEM transient thermal solver was employed to determine tissue temperature rise close to the implant caused by the heat sources. It requires knowing the relevant thermal properties of the tissues. The solver may approximately model blood perfusion, which is less important for bone, but is important for cardiac implants and other soft tissue implants [36].

The entire testbed has been integrated into Ansys Workbench, which allows the combination of different multiphysics modules within a single environment, as shown in Fig. 3.

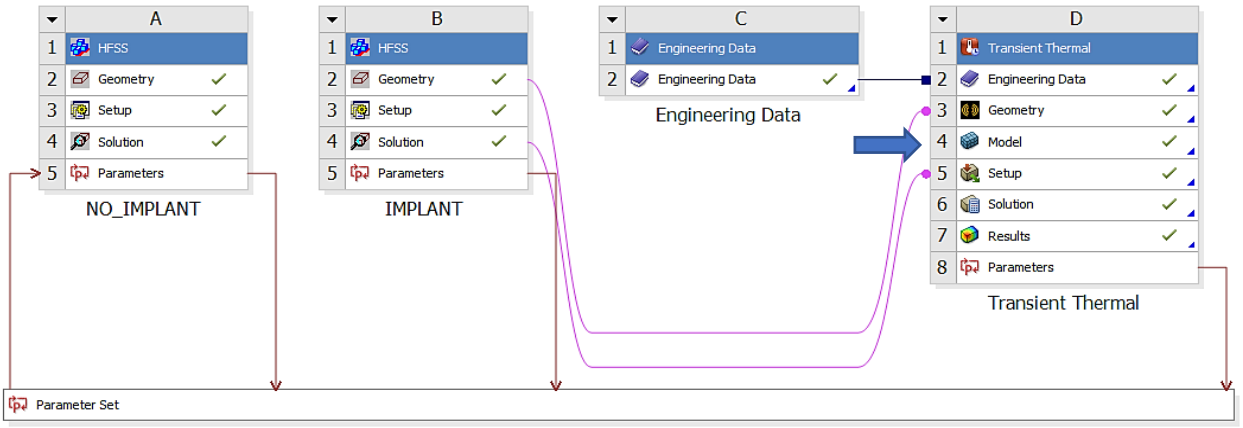

Fig. 3. Ansys Workbench modeling workflow consisting of the HFSS (electromagnetic) module labeled as A and B, and the transient thermal module labeled D. Thermal material properties are contained in module C.

bioRxiv preprint doi: https://doi.org/10.1101/2023.07.16.549234; this version posted July 18, 2023. The copyright holder for this preprint (which was not certified by peer review) is the author/funder. All rights reserved. No reuse allowed without permission.

In this way, the output of the electromagnetic solver (Figs. 3A and B) is the input to the thermal solver (Fig. 3D). Both accurate FEM solvers utilize the same human model geometry throughout, but with different material properties (thermal vs electromagnetic).

3. RESULTS

3.1 What is heating-related MR labeling of implants?

For the implantable devices that are categorized as MR Conditional, the labeling includes scan and rest times at a given whole-body SAR or $B_{1,rms}^{+}$ ("root mean square" value of B_1^+ averaged over a period of 10 seconds). This is described in the FDA's guidance document [5] (cf. also examples in [8]) where devices are to be labeled for a 1-hour MR session, including both scan and rest times. The guidance states a certain interleaving combination of scan (e.g., 5 min) and rest (e.g., 15 min) times that guarantees implant heating is less than 5 °C or another specified number [5]. The FDA-required procedure is a measurement test in an ASTM gel-based homogeneous phantom [5],[19]. When performing relevant numerical modeling, the pulse sequences and scan times should be converted to equivalent CW (continuous wave) operation, which is easier to model.

However, the response of the ASTM phantom is quite different from that of a real body, which includes bones and other tissues of varying electrical and thermal conductivities, as well as blood circulation and perfusion. In several test cases, our testbed prototype predicted a higher maximum temperature rise (up to 40% higher) at the implant tips versus *in-vitro* experiments with a simplified gel phantom. In other cases, and for other implants, however, the heating was substantially lower (by 50% or so). Therefore, the *in-silico* testbed will augment the ASTM measurements with accurate multiphysics modeling. Additionally, this modeling can assist with implant design in an efficient manner.

We note that this work is solely focused on the RF safety aspects of MR labeling. The results expressed herein should be considered supplemental to existing published guidelines.

3.2 Example: labeling long femoral titanium nail

Fig. 4 shows an example of testing results for a long titanium femoral nail subject to three cycles of 15 min with a 2.3 W/kg average equivalent SAR exposure followed by 5 minutes of rest, resulting in a 1-hour total exposure in a 1.5 T MRI coil. The model predicts that the temperature near the implant reaches 41 °C after the first exposure with its final value approaching 45 °C, a total increase of about 10 °C which is clearly unacceptable! Further simulations show that 4 min exposures followed by 16 min of rest would be a safe solution. In the testbed, the exposure time

bioRxiv preprint doi: https://doi.org/10.1101/2023.07.16.549234; this version posted July 18, 2023. The copyright holder for this preprint (which was not certified by peer review) is the author/funder. All rights reserved. No reuse allowed without permission.

is arbitrary and can be rapidly tested and adjusted (within 5-7 min) to meet the FDA requirements [5] and construct the proper MR exposure protocol.

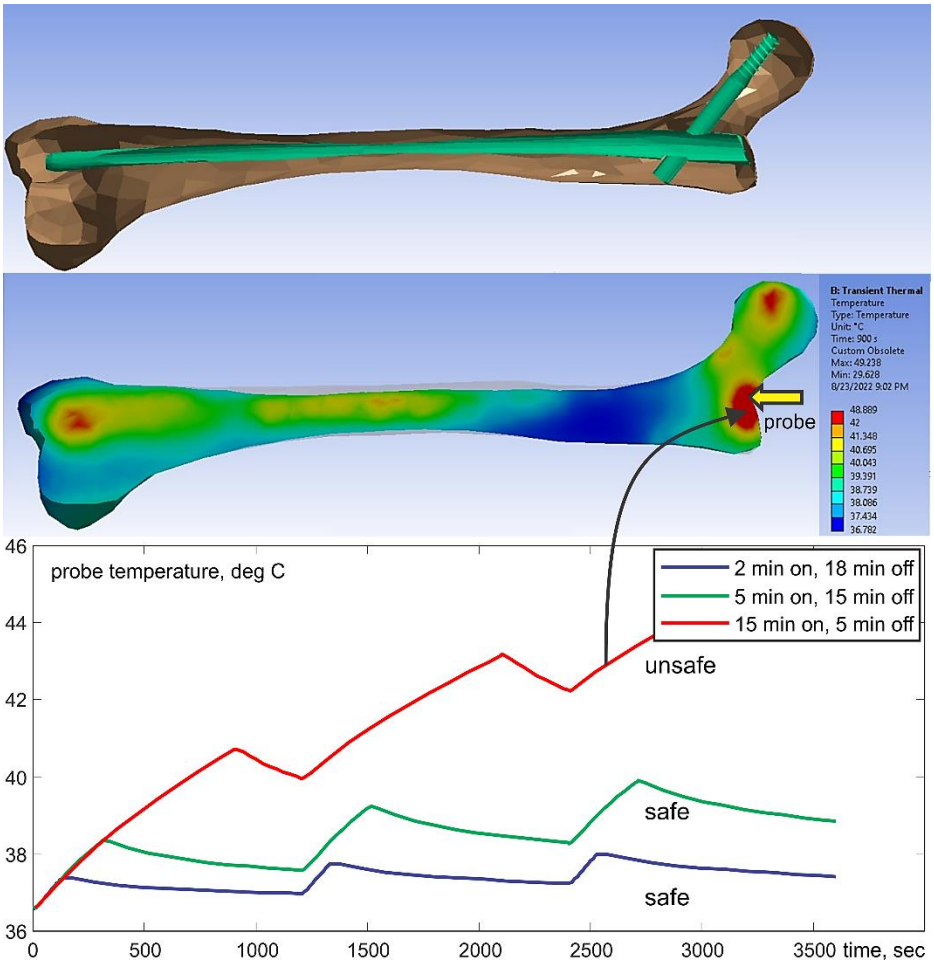

Fig. 4. Top – long femoral nail subject to three repetitions of 15 minutes exposure followed by 5 minutes of rest for 1 hour in total. Center – temperature contour plot in a cut plane roughly bisecting the embedded femoral implant at the end of the last heating cycle. Bottom – temperature rise profile at the temperature probe. Only the bone is shown but the computations are performed for the entire model.

3.3 Comparison with experiment for a long resonant metal conductor with a sharp tip

The most challenging and important cases correspond to testing large and potentially resonant metal implants [19] with relatively sharp tips or terminations since detecting resonance requires accurate high-frequency modeling. One extreme example was studied in Ref. [37], where a simulated percutaneous RF ablation surgical procedure using MR heating was performed in *ex-vivo* bovine liver in a 1.5 T scanner. The device under study was a bent long wire ‘antenna’ made resonant at the scanner Larmor frequency with an adjustable series capacitor. The antenna, a 26 AWG (0.40 mm) Teflon-insulated silver-plated copper wire taped around the edge of the patient table, was terminated in a simulated RF ablation needle (a 15 cm long 16 AWG/1.30 mm diameter bare copper wire), the tip of which was embedded into the liver to simulate the percutaneous

bioRxiv preprint doi: https://doi.org/10.1101/2023.07.16.549234; this version posted July 18, 2023. The copyright holder for this preprint (which was not certified by peer review) is the author/funder. All rights reserved. No reuse allowed without permission.

ablation of a solid hepatic tumor. The parametrized testbed coil model was used to replicate the RF antenna and needle geometry of Ref. [37], using standard electrical properties of human liver tissue. The peak tissue temperature increase imaged in Ref. [37] by the proton resonance frequency shift (PRFS) method (20 °C) and a 22 °C increase recorded by a fiber optic temperature sensor at the needle tip agreed well with our modeled prediction of a 23 °C increase using the modeling testbed.

A very fine FEM mesh resolution is required to accurately resolve temperature rise close to a sharp lead tip with a diameter of 1.3 mm – cf. Fig. 5. This is achieved using local automated adaptive FEM mesh refinement, which is a unique property of the present testbed. Fig. 5 shows the corresponding testbed setup along with the lesion. A few relevant field movies are available as supplementary materials [39].

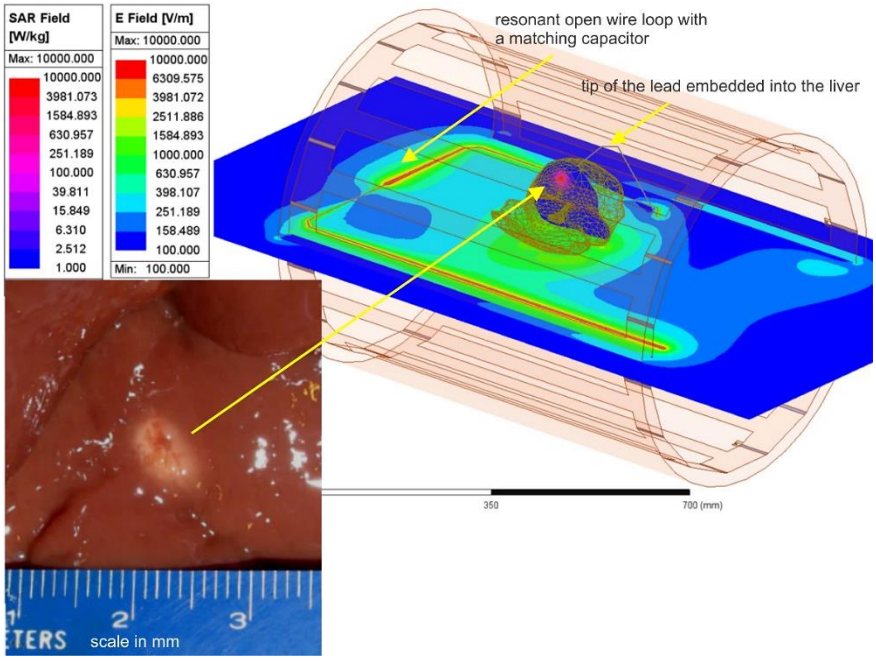

Fig. 5. Liver experiment setup: E-field distribution in the plane of the resonant loop and SAR distribution within liver in a plane passing through the tip of the lead. Bottom left – lesion in a section of *ex-vivo* bovine liver created with heating at the tip of a 16 gauge (1.3 mm) bare copper wire needle in about 1.5 min [37].

4. Discussion and Conclusion

The temperature rise in the surrounding tissues of a large orthopedic metallic implant subject to MR imaging is a significant point of concern and a potential barrier for the development of better implants. Numerical electromagnetic and thermal modeling offers a way to solve this complex problem with a sufficient degree of accuracy. We developed a complete testbed for realistic implant modeling, which includes a detailed FEM-compatible obese human female

bioRxiv preprint doi: https://doi.org/10.1101/2023.07.16.549234; this version posted July 18, 2023. The copyright holder for this preprint (which was not certified by peer review) is the author/funder. All rights reserved. No reuse allowed without permission.

model, a parameterized tunable generic MR coil model, a method for implant embedding, and an accurate radio frequency solver directly coupled with a transient thermal solver.

In the testbed, the MR exposure time is arbitrary and can be readily adjusted and rapidly tested (typically within ~5-7 min). This enables the user to meet regulatory requirements [5] and to construct a proper MR exposure protocol. A cross-platform compatibility of the *in-silico* model has been established previously [38]. Further validation of cross-platform electromagnetic and thermal coupling performance is currently underway with Dassault Systèmes CST Studio Suite software package. The testbed along with the open-source version of the human model VHP-Female College [13] is available online [39].

ACKNOWLEDGEMENTS

This work was supported by the National Institutes of Health grants R01AR075077 and R01EB029818.

References

[1]. Kanal E, Brown G., de Bruin PW, Kugel H. Scanning patients with MR conditional implants. *Philips Professional Healthcare*. *FieldStrength Article*. Dec. 2015. Online: https://www.usa.philips.com/healthcare/education-resources/publications/fieldstrength/mri-and-mr-conditional-implants.

[2]. Lim WY, Prabhu S, Schilling RJ. Implantable Cardiac Electronic Devices in the Elderly Population. *Arrhythm Electrophysiol Rev*. 2019 May;8(2):143-146. doi: 10.15420/aer.2019.3.4.

[3]. Puette JA, Malek R, Ellison MB. *Pacemaker*. [Updated 2022 Sep 12]. In: StatPearls [Internet]. Treasure Island (FL): StatPearls Publishing Co; 2022 Jan-. Available from: https://www.ncbi.nlm.nih.gov/books/NBK526001/

[4]. Brown JE, Qiang R, Stadnik PJ, et al. Calculation of MRI RF-Induced Voltages for Implanted Medical Devices Using Computational Human Models. 2019 Aug 28. In: Makarov S, Horner M, Noetscher G, editors. *Brain and Human Body Modeling*: Computational Human Modeling at EMBC 2018 [Internet]. Cham (CH): Springer; 2019. Chapter 14. Available from: https://www.ncbi.nlm.nih.gov/books/NBK549553/ doi: 10.1007/978-3-030-21293-3_1.

[5]. *Testing and Labeling Medical Devices for Safety in the Magnetic Resonance (MR) Environment*. U.S. Department of Health and Human Services, Food and Drug

bioRxiv preprint doi: https://doi.org/10.1101/2023.07.16.549234; this version posted July 18, 2023. The copyright holder for this preprint (which was not certified by peer review) is the author/funder. All rights reserved. No reuse allowed without permission.

Administration, Center for Devices and Radiological Health. May20th 2021. Online: https://www.fda.gov/media/74201/download.

[6]. *Understanding MRI Safety Labeling*. U.S. Food and Drug Administration. Summary, online: https://www.fda.gov/media/101221/download

[7]. American College of Radiology. ACR Manual on MR Safety. Version 1.0. 2020. ACR Committee on MR Safety. Online: https://www.acr.org/-/media/ACR/Files/Radiology-Safety/MR-Safety/Manual-on-MR-Safety.pdf

[8]. Shellock FG, Woods TO, Crues JV 3rd. MR labeling information for implants and devices: explanation of terminology. *Radiology*. 2009 Oct;253(1):26-30. doi: 10.1148/radiol.2531091030.

[9]. Fujimoto K, Smith A, Angelone LM, Dwivedi V, Rajan SS, Showalter BL, McMinn NL. Retrospective Analysis of Radio-frequency Safety of Orthopedic Passive Implantable Device. *Proc. Intl. Soc. Mag. Reson. Med*. 28 (2020). 4198. Online: https://cds.ismrm.org/protected/20MProceedings/PDFfiles/4198.html.

[10]. Medical Device Development Tool MDDT Q170004 Communications with FDA Center for Devices and Radiological Health, US Food and Drug Administration (FDA), Silver Spring, MD, United States. 2020-2022.

[11]. FDA MDDT: Computational Tool Comprising Visible Human Project® Based Anatomical Female CAD Model and Ansys HFSS/Mechanical® FEM Software for Temperature Rise Prediction near an Orthopedic Femoral Nail Implant during a 1.5 T MRI Scan. 03/30/32. *Neva Electromagnetics, LLC*. Online: https://www.fda.gov/media/166724/download. *U.S. Food and Drug Administration Bulletin of 03/30/2023*. Online: https://content.govdelivery.com/accounts/USFDA/bulletins/351ef58?reqfrom=share

[12]. FDA 510(k)/De Novo Clearance and Premarket Approval Applications: https://www.accessdata.fda.gov/scripts/cdrh/cfdocs/search/default.cfm, accessed Jan. 2023.

[13]. NEVA Electromagnetics, LLC. VHP-Female 2.2 (College). Online download page: https://www.nevaelectromagnetics.com/vhp-female-2-2

[14]. Fischbacher A, Borens O. Prosthetic-joint Infections: Mortality Over The Last 10 Years. J Bone Jt Infect. 2019 Sep 17;4(4):198-202. doi: 10.7150/jbji.35428.

bioRxiv preprint doi: https://doi.org/10.1101/2023.07.16.549234; this version posted July 18, 2023. The copyright holder for this preprint (which was not certified by peer review) is the author/funder. All rights reserved. No reuse allowed without permission.

[15]. Zanetti M. The Expanding Role of MRI in the Evaluation of Periprosthetic Hip Joint Infection. *Radiology*. 2020 Jul;296(1):109-110. doi: 10.1148/radiol.2020201419.

[16]. Li M, Glassman AH. What's New in Hip Replacement*. J Bone Joint Surg Am*. 2018 Sep 19;100(18):1616-1624. doi: 10.2106/JBJS.18.00583.

[17]. Neil P. Sheth, Jared R.H. Foran, William J. Peace. Joint Replacement Infection. *American Academy of Orthopaedic Surgeons*. Rosemont, Illinois, Feb. 2023. Online: https://orthoinfo.aaos.org/en/diseases--conditions/joint-replacement-infection/

[18]. Galley J, Sutter R, Stern C, Filli L, Rahm S, Pfirrmann CWA. Diagnosis of Periprosthetic Hip Joint Infection Using MRI with Metal Artifact Reduction at 1.5 T. Radiology. 2020 Jul;296(1):98-108. doi: 10.1148/radiol.2020191901.

[19]. Song T, Xu Z, Iacono MI, Angelone LM, Rajan S. Retrospective analysis of RF heating measurements of passive medical implants. *Magn Reson Med*. 2018 Dec;80(6):2726-2730. doi: 10.1002/mrm.27346.

[20]. Al-Dayeh L, Rahman M, Venook R. Practical Aspects of MR Imaging Safety Test Methods for MR Conditional Active Implantable Medical Devices. *Magn Reson Imaging Clin N Am*. 2020 Nov;28(4):559-571. doi: 10.1016/j.mric.2020.07.008.

[21]. Arduino A, Baruffaldi F, Bottauscio O, Chiampi M, Martinez JA, Zanovello U, Zilberti L. Computational dosimetry in MRI in presence of hip, knee or shoulder implants: do we need accurate surgery models*? Phys Med Biol.* 2022 Dec 15;67(24). doi: 10.1088/1361-6560/aca5e6.

[22]. Arduino A, Zanovello U, Hand J, Zilberti L, Brühl R, Chiampi M, Bottauscio O. Heating of hip joint implants in MRI: The combined effect of RF and switched-gradient fields. *Magn Reson Med.* 2021 Jun;85(6):3447-3462. doi: 10.1002/mrm.28666.

[23]. Bassen H, Zaidi T. Parameters Affecting Worst-Case Gradient-Field Heating of Passive Conductive Implants. *J Magn Reson Imaging*. 2022 Oct;56(4):1197-1204. doi: 10.1002/jmri.28321.

[24]. Wooldridge J, Arduino A, Zilberti L, Zanovello U, Chiampi M, Clementi V, Bottauscio O. Gradient coil and radiofrequency induced heating of orthopaedic implants in MRI: influencing factors. *Phys Med Biol.* 2021 Dec 23;66(24). doi: 10.1088/1361-6560/ac3eab.

bioRxiv preprint doi: https://doi.org/10.1101/2023.07.16.549234; this version posted July 18, 2023. The copyright holder for this preprint (which was not certified by peer review) is the author/funder. All rights reserved. No reuse allowed without permission.

[25]. Winter L, Seifert F, Zilberti L, Murbach M, Ittermann B. MRI-Related Heating of Implants and Devices: A Review. *J Magn Reson Imaging*. 2021 Jun;53(6):1646-1665. doi: 10.1002/jmri.27194.

[26]. Oberle M. MDDT Summary of Evidence and Basis of Qualification Decision for IMANALYTICS with MRIXVIP1.5T/3.0T and BCLIB. ZMT Zurich MedTech AG, Zurich, Switzerland. 12/4/2020. *FDA. Doc ID 01147.02.00.* US Food and Drug Administration (FDA); 2021. https://www.fda.gov/media/148922/download Accessed Jan. 2023.

[27]. Makarov SN, Noetscher GM, Yanamadala J, Piazza MW, Louie S, Prokop A, Nazarian A, Nummenmaa A. Virtual Human Models for Electromagnetic Studies and Their Applications. *IEEE Rev Biomed Eng*. 2017;10:95-121. doi: 10.1109/RBME.2017.2722420.

[28]. Noetscher, G., Serano, P., Nazarian, A., Makarov, S. (2023). Computational Tool Comprising Visible Human Project® Based Anatomical Female CAD Model and Ansys HFSS/Mechanical® FEM Software for Temperature Rise Prediction Near an Orthopedic Femoral Nail Implant During a 1.5T MRI Scan. In: Makarov, S., Noetscher, G., Nummenmaa, A. (eds) *Brain and Human Body Modelling* 2021. Springer, Cham. https://doi.org/10.1007/978-3-031-15451-5_9

[29]. Gosselin MC, Neufeld E, Moser H, Huber E, Farcito S, Gerber L, Jedensjö M, Hilber I, Di Gennaro F, Lloyd B, Cherubini E, Szczerba D, Kainz W, Kuster N. Development of a new generation of high-resolution anatomical models for medical device evaluation: the Virtual Population 3.0. *Phys Med Biol.* 2014 Sep 21;59(18):5287-303. doi: 10.1088/0031-9155/59/18/5287. Online: https://itis.swiss/virtual-population/virtual-population/overview/

[30]. IT'IS Foundation. Three Class III Obese ViP Models for Improved Patient Coverage. Jan. 31st 2023. Online: https://itis.swiss/news-events/news/virtual-population/class-iii-obese-models/

[31]. Noetscher GM, Serano P, Wartman WA, Fujimoto K, Makarov SN. Visible Human Project® female surface based computational phantom (Nelly) for radio-frequency safety evaluation in MRI coils. *PLoS One*. 2021 Dec 10;16(12):e0260922. doi: 10.1371/journal.pone.0260922.

[32]. Noetscher, G.M. (2021). The CAD-Compatible VHP-Male Computational Phantom. In: Makarov, S.N., Noetscher, G.M., Nummenmaa, A. (eds) *Brain and Human Body Modeling 2020*. Springer, Cham. https://doi.org/10.1007/978-3-030-45623-8_19.

bioRxiv preprint doi: https://doi.org/10.1101/2023.07.16.549234; this version posted July 18, 2023. The copyright holder for this preprint (which was not certified by peer review) is the author/funder. All rights reserved. No reuse allowed without permission.

[33]. Kozlov M, Noetscher GM, Nazarian A, Makarov SN. Comparative analysis of different hip implants within a realistic human model located inside a 1.5T MRI whole body RF coil. *Annu Int Conf IEEE Eng Med Biol Soc.* 2015;2015:7913-6. doi: 10.1109/EMBC.2015.7320227.

[34]. V. Spitzer, M. J. Ackerman, A. L. Scherzinger, and D. W. Whitlock, "The visible human male: A technical report," J. Amer. Medical Informatics Assoc., vol. 3, no. 2, pp.118-130, 1996.

[35]. M. J. Ackerman, "The Visible Human Project," Proc. IEEE, vol. 86, no. 3, pp. 504-511, Mar. 1998. Available: https://www.nlm.nih.gov/research/visible/visible_human.html.

[36]. Winter L, Seifert F, Zilberti L, Murbach M, Ittermann B. MRI-Related Heating of Implants and Devices: A Review. *J Magn Reson Imaging*. 2021 Jun;53(6):1646-1665. doi: 10.1002/jmri.27194.

[37]. Hue YK, Guimaraes AR, Cohen O, Nevo E, Roth A, Ackerman JL. Magnetic Resonance Mediated Radiofrequency Ablation. *IEEE Trans Med Imaging*. 2018 Feb;37(2):417-427. doi: 10.1109/TMI.2017.2753739.

[38]. Yanamadala J, Noetscher GM, Louie S, Prokop A, Kozlov M, Nazarian A, Makarov S. Multi-Purpose VHP-Female Version 3.0 Cross-Platform Computational Human Model. *Proceedings of the 10th European Conference on Antennas and Propagation*; 2016 Apr 10–15; Davos, CH.

[39]. Online Dropbox link: In-Silico Testbed for MR Labeling of Orthopaedic Implants based on open-source VHP-Female 2.2 College. June 2023.